Research Square

Preprints are preliminary reports that have not undergone peer review.
They should not be considered conclusive, used to inform clinical practice,
or referenced by the media as validated information.

The improvement on foaming properties of soybean protein isolates via interaction with β-D-glucan and myricetin: In an interfacial perspective

Junsheng Li
Yunnan Provincial Academy of Food and Oil Science
Dan Lei
National R&D Center for Se-rich Agricultural Products Processing, Wuhan Polytechnic University
Yunman Wen
Yunnan Provincial Academy of Food and Oil Science
Xuheng Nie
Yunnan Provincial Academy of Food and Oil Science
Shuyi Li
lishuyisz@sina.com
National R&D Center for Se-rich Agricultural Products Processing, Wuhan Polytechnic University

Research Article

Keywords: Complexes, Foam morphology, Foaming properties, Dilatational rheology, Adsorption kinetics

Posted Date: November 26th, 2026

DOI: https://doi.org/10.21203/rs.3.rs-11788508/v1

License: This work is licensed under a Creative Commons Attribution 4.0 International License.
Read Full License

Additional Declarations: No competing interests reported.

Abstract

A series of binary and ternary complexes prepared by myricetin (MC), β-D-glucan (DG), and soybean protein isolate (SPI) were investigated by the foam morphology, foaming properties after heating and dilatational rheology. The results showed that foams of ternary complexes were more uniform in size distribution compared with SPI from 30 s to 1800 s evolution, among which SPI-MC-DG complex was most regular, indicating their excellent foam properties. Then, the all complexes at 25°C had significant differences (p<0.01) in foam ability (FA) compared with SPI, in which SPI-MC got best FA for 675% than the ternary complexes. The surface dilatational rheology results especially the surface tension, expansion modulus and elastic modulus showed that the foaming properties of SPI-MC and SPI-MC-DG were better than other complexes. The adsorption kinetics was diffusion adsorption, also the addition of MC and DG into SPI would promote penetration and rearrangement.

1 Introduction

Proteins from soybeans have been used in a wide variety of food products and as a major alternative to animal-source proteins, among which the SPI is widely used in beverages, dairy, pasta and meat-substitute industries because of their functional properties such as foaming, emulsification and gelation (Azizi, Baggio, Capuano, & Pellegrini, 2024). Foam is a system in which the liquid phase surrounds the gas phase. Foam is widely used in foam foods such as cream, ice cream and cake (X. Li, Murray, Yang, & Sarkar, 2020). Researches showed that proteins have the capacity of adsorbing and unfurling at the air-water interface, which further improve the viscoelastic property of interface films and stability of the formed foam (Q. Jin, Li, Cai, Zhang, Yadav, & Zhang, 2017). For example, milk proteins (casein and whey proteins) and egg proteins (ovalbumin and lysozyme) are both used in the food system due to their good foaming properties (Jurado Gonzalez & Sörensen, 2020). The critical factors affecting the quality of foamy foods are foaming capacity and foaming stability (FS), interface expansion rheological ability. However, naturally occurring SPI does not have ideal foaming and foam stabilization abilities due to it contains more rigid structures, which faces limitations in foaming capacity despite their industrial potential (Q. Yang, Yang, Waterink, Venema, de Vries, & Sagis, 2024).

It was studied that polysaccharides, polyphenols and proteins interacted with each other to alter the structure of the protein, resulting in changes in the interfacial properties of the protein. Since polyphenols are easily oxidized into quinones, which can covalently react with nucleophilic molecules, polyphenols are highly reactive and can interact with various compounds (C. Yang, Wang, Wang, Xia, & Wu, 2019). According to (Rawel, Czajka, Rohn, and Kroll, 2002), the interaction between phenolic compounds the interaction between phenolic compounds and proteins changes the secondary and tertiary structures of proteins and affects the interfacial properties of molecules such as FA. The whey protein isolate and DG soluble complex reduce air-water interface tension, exhibiting high adsorption quality, and forming a dense, rigid interface layer, exhibiting superior foam characteristics (Hu, Xu, Jiang, & Hou, 2025).

SPI is modified with polysaccharides and polyphenols to prepare a natural emulsifier with antioxidant capacity, with excellent antioxidant capacity and emulsifying property, making it suitable for emulsion delivery systems (Ke & Li, 2024). Nanoparticles prepared by SPI-oat β-glucan (OG) extrudates (E-SPI-OG) can encapsulate quercetin to improve solubility and its bioaccessibility (J. Li & Li, 2025).

Recently, ternary complexes of SPI, DG and MC binding by covalent or non-covalent are prepared in our laboratory, which also can be used to construct emulsion delivery system with high stability and environmental resistance (Jian, Li, Zhu, Zhang, Deng, & Cravotto, 2023). Also, the ternary complexes can enhance the stability and bioavailability of β-carotene emulsions, providing a basis for developing functional foods utilizing protein resources. Previous research has demonstrated the superior emulsifying activity of the covalent complexes SPI-DG-MC (Luo et al., 2025).

Based on the prepared of SPI, DG and MC binary and ternary complexes, we aim to explore foam morphology of all complexes, foaming properties under different heating conditions, then try to verify and interpret the foaming mechanism of complexes by interfacial rheological ability, which helps to further illustrate the beneficial effect of binary and ternary and provide a theoretical basis for the study of functional properties in foaming food systems.

2 Materials and methods

2.1 Materials and chemicals

Soybean protein isolate (SPI, ≥ 96.0%, CAS: 9010-10-0, Lot: 20201016) was purchased from Henan Zhongtai food chemical Co., LTD. β-glucan (DG) was derived from barley (≥ 95.0%, CAS: 9041-22-9, Lot: 20210306), purchased from Shanghai Yuanye Biotechnology Co., LTD. Myricetin (MC, HPLC ≥ 98.0%, CAS: 529-44-2, Lot: 200619) was purchased from Shandong West Asia Chemical Co., LTD. All other chemical reagents are analytically pure and purchased from Sinopharm Chemical Reagents Co., LTD.

2.2 Preparation of binary and ternary complexes

The SPI solution was magnetically stirred at room temperature (20°C) for 12 h, followed by centrifuged at 9000 rpm for 30 min, and the supernatant was stored at 4°C for later use. DG solution (2 mg/mL) was magnetically stirred at 80°C for 2 h for reserve use. MC solution (2.5 mg/mL) was prepared for later use. The preparation of ternary complexes followed the method of W. Yang, Xu, Liu, Sun, Yuan, et al (2015) with appropriate modifications. According to different addition order, the above spare solutions were prepared into ternary complexes. Subsequently, the binary complexes of SPI-DG, SPI-MC and DG-MC were prepared using the same stock solution.

2.3 Foam morphology

A small amount of foam was taken 2 ~ 3 cm from the bottom of the plastic beaker, then gently apply it to the slide, which is then covered with a cover glass and fixed on the sample stage. The foam morphology from 30 s to 30 min was observed using a microscope (Axioskop 40, ZEISS, Germany).

2.4 Foaming properties

The foamability and foam stability of the compound were determined according to the method of Peng, Yang, Li, Tang, and Li (2017) with some modifications. Briefly, the samples (15 mL) were heated in a water bath at 25°C, 60°C, and 80°C for 20 min, respectively. All samples were then homogenized at room temperature (25°C) at 8000 rpm for 2 min using a homogenizer (T18, IKA, Germany) and immediately transferred into a measuring cylinder. The time function of foam volume and liquid volume was then recorded. The foamability (FA) was expressed as a percentage of the foam volume at 2 min (V_2) and the initial liquid volume of the sample (15 mL).

$$\mathrm{FA}\ (\%) = \frac{\mathrm{V_2}}{15} \times 100$$

1

The foam stability (FS) was measured by recording the half-life ($t^{1/2}$), which was the time it taken the foam volume to reduce to half the initial foam volume. The rate at which the liquid was discharged from the foam was determined by recording the volume of the liquid as a function of time.

2.5 Surface dilatational rheology

2.5.1 Surface tension measurement

The dynamic surface tension of samples was measured according to the method of Peng, Yang, et al. (2017) using a suspended drop interfacial rheometer (DSA30S, KRÜSS Scientific, Germany). An axisymmetric drop is formed through a syringe system and photographed by a camera. The sample was filled into a 0.5 mL syringe using a 1.8 mm diameter needle with a suspended drop volume of 16 μL and then placed into a 5 mL sample pool to monitor the dynamic surface tension for 3 h.

2.5.2 Time sweep

The surface elastic modulus (E_d) is a function of time (t) with an amplitude of 10% and a frequency of 0.05 Hz for 3 h. The scan alternately goes through 5 sinusoidal oscillation cycles and 5 static oscillation cycles.

2.5.3 Amplitude sweep

Amplitude sweep was performed after the sample was balanced for 3 h, and the amplitude ranged from 5% to 100% at a constant frequency of 0.05 Hz. All experiments were conducted at 20℃.

2.5.4 Frequency sweep

Frequency scanning was performed after the surface tension test. The amplitude was 10% and the frequency is 0.01 ~ 0.1Hz. The slope of the linear fit between the double logarithm of the frequency and the surface dilatational modulus (E) reflected the frequency dependence.

2.5.5 Adsorption kinetics

The effect of DG and MC on the adsorption behavior of protein molecules was analyzed by measuring the diffusion, penetration and rearrangement of protein to the interface. The surface tension (γ) was calculated by analyzing the shape of the suspended drop according to the Gauss-Laplace equation. The interfacial pressure (π) at the air-water interface of the sample is calculated according to Eq. (2):

$$\pi = \gamma_0 - \gamma \#(2)$$

where γ is sample interfacial tension air-water interface, γ_0 is the interfacial tension of air-ultrapure water 72 ± 0.1 mN /m).

The adsorption behavior of protein at low interfacial layer concentration is affected by diffusion. Diffusion rate (K_{diff}) is the slope of the curve of interfacial pressure (π) and adsorption time ($t^{1/2}$), which could be calculated by an improved form of the Ward and Tordai models (Eq. (3)) (Pérez, Sánchez, Pilosof, & Rodríguez Patino, 2008):

$$\pi = 2C_0 kT \left(D \bullet \frac{\theta}{3.14} \right)^{\frac{1}{2}} \#(3)$$

where *k* is the Boltzmann constant, *T* is the absolute temperature, C_0 is the concentration of the continuous phase, and *D* is the diffusion coefficient.

The adsorption behavior of protein at high interfacial layer concentration is determined by the infiltration and rearrangement of protein molecules in the adsorption layer. The penetration rate and molecular recombination rate of proteins at the interface layer were analyzed according to Eq. (4):

$$\ln \left[\frac{\pi_a - \pi_b}{\pi_a - \pi_0} \right] = -k_i t (4)$$

where π_a, π_0 and π_b represent the final adsorption time, the initial time, and the interfacial pressure at any time t, respectively, and k_i is the rate constant. The permeability rate constant (K_P) and molecular rearrangement rate constant (K_R) correspond to the initial slope and the second slope respectively.

2.6 Statistical analysis

All data was provided as mean ± standard deviations (SD), and analysis of variance. The measurements for each parameter were taken three times. One-way analysis of variance (ANOVA) was used to determine the significance of the difference between the mean values of $P < 0.05$. Origin 2018 (Origin-Lab, Northampton, MA, USA) software was utilized for data processing and chart plotting.

3 Results and discussion

3.1 Foam morphology of different complexes

Foaming performance was closely related to the bubble size and uniform protein distribution (Wang et al., 2024). It was studied that the initial bubbles of complexes were smaller and more uniform in size distribution, as well as more regular in shape (tend to be round), compared with SPI, indicating their excellent FA (Peng, Jin, et al., 2017). The evolutions of foam sizes with time for different complexes were demonstrated in Fig. 1 that the initial bubble shapes regularity and distributions of ternary foaming were more regular than SPI, which second were the binary. With the extension of time (30 s-1800 s), the bubbles size of all complexes increased gradually and the shapes of foam began to change from circular to polygon. This were because of the destabilizing processes, such as liquid drainage, coarsening, and coalescence (Wan, Yang, & Sagis, 2016a). As could be seen Fig. 1, the bubbles shape evolutions were consistent with that of Wan's conclusion, that the shapes became polygon from circular from 30 s to 1800 s. Among the ternary complexes, the foam shapes of SPI-MC-DG were still more regular, more consistent and the size distribution was more uniform during the entire process, indicating the best FS.

3.2 Foam properties of different complexes after heat-treated

As a typical thermodynamically unstable system, gas-liquid in the foam interface has high surface free energy and interface area and The spontaneous reduction of free energy leads to drainage of liquid, coalescence and disproportionation, coarsening (Briceño-Ahumada & Langevin, 2017). FA and FS were used to represent foaming properties and the foam properties could be indicated by the initial foam volume and bubble size, where the larger amount foam and smaller bubble size indicate the better foam properties (Peng et al., 2018).

The foam volume and liquid volume in the foam were recorded after different binary complexes and ternary complexes were prepared then heated in water bath at 25 ℃, 60 ℃ and 80 ℃ for 20 min in Fig. 2., respectively. Foam volume (Fig. 2 (a-i)) and liquid volume (Fig. 2 (b-j)) in the foam were recorded and calculated into the FA (%) in Fig. 2 (c-k), horizontally. which showed significant difference ($p < 0.01$). It was shown in Fig. 2 that different complexes did have distinction on the foam properties showing in (especially between the binary and ternary). In Fig. 2. (a, e, i), the initial foam volume of SPI-MC was larger than others at 25°C, but when the temperature increased from 25°C to 80°C, it gradually presented a more obvious trend that the final foam volume of SPI-MC was the largest and SPI-DG was smallest, indicating the best and worst FA, while the ternary complexes nearly had not difference. The volume of foam liquid results in Fig. 2. (b, f, j) were basically the same as that foam volume results. It was shown in Fig. 2 that different complexes did have distinction on the foam properties showing in (especially between the binary and ternary). It was also demonstrated that varied raw material had a direct effect on the structural features of ternary complexes produced by proteins, polysaccharides, and polyphenols (W. Yang et al. (2015). As seen in Fig. 2. (c, g, k), at 25°C, the FA of SPI-MC (675%) was significantly higher than that of the ternary complexes ($p < 0.01$). This might contribute to that the interaction between

polyphenols and proteins might enhance the intermolecular interaction thus improving the foam properties of system(Zhan, Li, Wang, Shi, Li, & Sheng, 2018). When the temperature increased, the FA of SPI-MC remained significantly higher than other complexes, but the difference between the ternary complexes and other complex gradually showed nearly no difference as well as SPI, indicating that temperature had an impact on the FA of the complexes. The conclusion was similar to the FA results of gliadin nanoparticles affected by temperature after heating from 20°C to 70°C (Penget al. (2018).

With the addition of polyphenols, the role of bridging between proteins and proteins was conducive to multilayered protein membranes develop at the interface (Zhan, Li, et al., 2018). The instability of foams might be due to the drying of the foam caused by drainage of liquid, and the rupture of the bubble film and polymerization into a large bubble. Meanwhile, the transfer of gas from small bubbles to large bubbles causes foam disproportionation, leading to foam instability and volume reduction. As depicted in Fig. 2(a), the FS also could be measured by the Half-life time (t1/2) and the longer the half-life time, the better the FS (Peng et al. (2018). The half-life time (t1/2) of the ternary complexes and SPI-MC was significantly longer than SPI-DG and SPI seen in Fig. 2 (d, h, l) ($p < 0.01$) indicating better FS. The ranking of half-life time (t1/2) also the FS were SPI-DG-MC > SPI-MC-D > SPI-MC > DG-MC-SPI > SPI> SPI-DG, which might be because most of the binding sites were occupied when SPI reacted and formed a complex, resulting in insufficient binding sites to react with the complex when DG and MC were introduced (Lei et al., 2022) ($p < 0.01$).

3.3 Surface adsorption behavior

3.3.1 Surface tension measurement of different complexes

The foam properties were depended on the protein adsorption capacity at the air-water interface, the contact rheological characteristics and the rate of gas diffusion in the foam, as a complicated phenomenon (Zhan, Li, et al., 2018). The diffusion adsorption of protein molecules at the air-water interface was be characterized by dynamic surface tension to study the foam properties (Foegeding, Luck, & Davis, 2006). Referring to the curve of interface pressure could approximately be divided into three stages: induction period, rapid decreased period and slow decreased period. It was in Fig. 3 showed the surface tension of different samples adsorbed at air/water interface in 11000 s that the surface tension dramatically dropped within the about 400 s, indicating a rapid adsorption of all complexes at the interface during the induction period. Following the induction period, the interfacial pressure of all samples dropped fast to a specific value before 2000 s, then, gradually decreased to a saturation point, implying that the interface has been saturated by adsorption(Dombrowski, Gschwendtner, & Kulozik, 2017; Peng, Yang, et al., 2017). However, the surface tension steadily reduced and became reasonably steady from 2000 s to 11000 s. There might be a positive correlation between surface tension and the foaming properties. Furthermore, adsorption rates were observed at different complexes, among which SPI-MC and SPI-MC-DG had the quickest rate of decreasing surface tension, demonstrating a rapid adsorption at the interface and a high surface-active property, resulting better foam properties (Peng, Yang, et al., 2017). This result was consistent with prior findings about foam

properties (Fig. 1), which might be related to the surface properties of complexes and the macroscopic behavior of bubbles.

3.3.2 Time sweep of different complexes

E_d at flow points were determined as the most important parameters predicting tactile sensory modalities on large deformation (spooning) such as scoopability, creaminess and gumminess. The Ed was a measurement of the energy storage property of the emulsion, which deformed and returned to its original state, determined the emulsion support and stability. The E was a measurement of energy loss that occurred when the emulsion deformed and flowed internally, experiencing internal friction, which determined smoothness and adhesiveness of the emulsion (Musollini et al., 2026). Research about foaming properties, linear and nonlinear surface dilatational rheology of sodium caseinate, tannin acid and octenyl succinate starch ternary complexes had shown that the greater the surface dilatational modulus, the better the FS (Zhan, Li, Shi, Wu, & Li, 2019).

The surface dilatational modulus (*E*d) and surface elastic modulus (*E*) of different complexes as a function of time was shown in Fig. 4(a) and (b), respectively. As shown in the Fig. 4(a), around the 2000 s, a linear decrease indicated that the structure of the emulsion temporarily destroyed after shearing. Afterward, a linear rebound suggested that the structure of the liquid was self-healing. The rebound rate in the Fig. 4 was SPI-MC > SPI-MC-DG> other composites, and the greater the rebound rate, the better the foaming properties of the SPI emulsion. This was probably because the addition of MC might have promoted the formation of a three-dimensional structure between SPI molecules, reducing the loss of internal friction energy, affecting the magnitude of the *E*d (Zhan, Li, et al., 2018).

Besides, The SPI-MC and SPI-MC-DG were higher *Ed* compared to SPI indicated their higher viscoelasticity at the air/water interface layer, which might account for the better foam properties (Xiong et al., 2016). The most significant effect was consistent with Zhan, Li, et al. (2018). In addition, the results of *E* were consistent with *Ed*, that the higher values, the better the FS (Zhan, Li, Youssef, & Li, 2021). The *E* of both binary and ternary complexes were higher than that of SPI (Fig. 4(b)), implying that the presence of MC and DG might had a synergistic effect on the elasticity of the protein membrane, which further enhanced the connectivity of the interfacial protein network and improved the FS of SPI (Maldonado-Valderrama & Patino, 2010; Peng, Jin, et al., 2017).

3.3.3 Frequency sweep of different complexes

Frequency scanning was performed on the adsorption interface to further understand the surface rheological properties of the adsorption interface layer with a frequency set at 0.01 ~ 0.1 Hz and a fixed amplitude of 10% shown in Fig. 5(a). The elastic adsorption layer around the bubbles on the surface was formed when tannic acid was added into casein, resulting with the tension pressure and expansion modulus also increased significantly. For all complexes, *E* increased with frequency, it may be related to the dynamic exchange behavior and structural rearrangement of complexes at the air/water interface (W. Jin, Zhu, Jiang, Shao, Li, & Huang, 2017).

The slope of the linear fit of log (Ed) and log (frequency) was shown in Fig. 5(b), the magnitude of the slope reflected response sensitivity of the liquid to the scanning frequency. Then the linearly fitted slope column chart was performed with significance analysis in Fig. 5(b). The slope was less than 1, indicating that the viscosity was in a secondary position, and the internal formation of the liquid three different dimensional network structure was extremely strong, restricting the viscous flow. The greater the slope, the weaker the constraint of the liquid elastic structure and the stronger the FA were. When the slope was closely to 0.5, the elastic behavior of the interface layer was affected by the diffusion rate of surfactant in solution to the interface layer according to the model of (Peng, Yang, et al., 2017).

As shown in Fig. 5(b), all samples had slopes less than 0.5 and exhibited an elastic response. SPI-MC-DG and SPI-DG-MC were significantly larger than other samples indicating that elastic behavior was weakly constrained and better FA. This result did agree with that of foam properties (Fig. 1).

3.3.4 Amplitude sweep of different complexes

Foam flow tests showed that surface dilatational modulus had decisive effect on produced foam size, which partially determined foam flow pressure drop and the FS. Small amplitude oscillatory frequency sweeps gave structure sensitive information that enabled the characterization of the structure rheologically (Le, Erturk, & Kokini, 2023).

To evaluate the deformation degree of complexes under different amplitude and interfacial rheology, the *E* of complexes was determined with a constant frequency of 0.1 Hz and the amplitude range from 5% to 30%. The key point of *E* and amplitude curve was to determine whether there was a linear viscoelastic zone, to judge the structural stability and shear resistance of emulsion. Generally, the *E* was basically flat in the low amplitude (< 10%), indicating that the emulsion structure had not been destroyed and the elasticity was stable. When the amplitude exceeded (30%), the elastic modulus decreased significantly, and the three-dimensional structure and particle stacking structure inside the emulsion areared and destroyed. Amplitude at 30% was the yield point, the greater the yield point of the emulsion, the stronger its shear resistance, and the better its stability (Kovalchuk, Aksenenko, Trukhin, Makievski, Fainerman, &Miller, 2018; Wan et al., 2016a; Wan, Yang, & Sagis, 2016b). As shown in Fig. 6, the E value changed little when the amplitude was less than 15%, indicating that there was a linear viscoelastic zone, and the yield point of all samples was 15%, indicating that the overall stability of the lotion had little difference. However, in terms of elastic modulus values, the stability of overall ternary complexes was stronger than that of binary complexes. The lower *E* values showed instability of foam which attributed to the influence of small molecule diffusion on the elastic response of the interface to the amplitude of complexes. The conclusion consisted of the FS in Fig. 2.

3.3.5 Adsorption kinetics of different complexes

The adsorption type of protein included diffusion adsorption and kinetic adsorption which could be explained when the diffusion rate of protein molecules from the main phase was slower than the kinetic

process on the interface layer, it was called diffusion adsorption. Otherwise, it was kinetic adsorption (Bos & Vliet, 2001).

The ethanol soluble components in wheat aqueous phase protein showed a higher initial surface pressure, indicating stronger surface activity and consequently, superior FA (Zhao et al., 2024). As shown in Fig. 7 (a) was the curves of interfical pressure and time, among which the highest initial surface pressure value the first point SPI-MC-DG, secondly was SPI-MC, indicating the complexes were better activity and FA than other complexes. The adsorption behavior of protein at low interface layer concentration was affected by diffusion whose curve of interface pressure and time which could be roughly divided into three stages: induction period, rapid growth period and slow growth period (Zhan, Li, et al., 2018). As could be seen in Fig. 7(a) that effect of different complexes on the interfacial pressure as time extended at the air-water interface was measured and the slope in induction period was also indicated the FA. The SPI-MC-DG grew the fastest when compared to other complexes and eventually reached a highest steady interfacial pressure value, showing the strongest surface activity and FA, secondly was the SPI-MC binary.

The adsorption process of protein was consisted of three stages: (1) the molecular diffusion from the body phase to the interface for adsorption; (2) The molecules undergo penetration and rearrangement under the drive of interfacial tension; (3) molecules aggregate and rearrange at the interface to balance the interfacial tension and form an interfacial film (Talansier, Loisel, Dellavalle, Desrumaux, Lechevalier, & Legrand, 2009). It was shown in Fig. 7(b), the adsorption type was diffusion adsorption. The diffusion coefficient (*Kdiff*) of protein molecules from the main phase to the interface was shown in Table 1. Research had indicated that the FA of protein was positive correlate to the initial *Kdiff* at the air-water interface (Patino, Sánchez, Ortiz, Niño, & Añón, 2004). The *Kdiff* of the ternary complexes and SPI-MC were higher than that of SPI-DG and SPI and the *Kdiff* was observed in SPI-MC-DG (*Kdiff* = 0.49), SPI-MC (*Kdiff* = 0.44), showing the best FA of SPI-MC-DG, secondly was SPI-MC, besides, indicating that the addition of MC into SPI might improve the FA of SPI. Whereas, the *Kdiff* of DG-MC-SPI, SPI-DG-MC and SPI-DG were 0.33, 0.31 and 0.28, respectively, whose diffusion were suppressed compared with SPI-MC-DG and SPI-MC, suggesting that addition into DG before MC might affect the molecule diffusion, Similar research was reported that the protein-polyphenol interactions might influence protein flexibility and essential protein conformational shift to insert in the interface (von Staszewski, Pizones Ruiz-Henestrosa, & Pilosof, 2014). Also, the addition of MC would affect the binding sites and binding constants of SPI molecule.

Table 1
Diffuse rate (*Kdiff*), structure unfolding (K_P), rearrangement (K_R) for different compounds at the air-water interface (The numbers in parentheses represent the fitting coefficients R^2).

K_{diff}	SPI	SPI-DG	SPI-MC	DG-MC-SPI	SPI-MC-DG	SPI-DG-MC
	0.24 (1.00)	**0.28 (1.00)**	**0.44 (0.95)**	**0.33 (0.99)**	**0.49 (0.97)**	**0.31 (1.00)**
K_P ($\times 10^{-4}$)	2.67 (0.98)	2.96 (0.98)	3.08 (0.98)	3.20 (0.97)	3.11 (0.98)	2.88 (0.98)
K_R ($\times 10^{-4}$)	1.80 (0.98)	1.89 (0.94)	1.91 (0.96)	1.95 (0.94)	1.93 (0.96)	1.92 (0.98)

As shown from curves in Fig. 3(c), the penetration and rearrangement process of SPI could be roughly divided into two stages: steadily decreased in the early stage and dropped quickly in the later stage, whose curve slopes represented the penetration rate (*KP*) and the rate of rearrangement (*KR*) (Perez, Carrara, Sánchez, Santiago, & Rodríguez Patino, 2009), respectively, which the results were shown in Table 1. The *Kdiff* of the complexes was significantly higher than that of SPI, indicating that the modification of protein molecules by MC and DG was conducive to faster diffusion and penetration from the main phase to the interface layer. Besides, the values showed the same trends between KP with the K*R* that complexes penetrated and rearranged faster than SPI, in which the DG-MC-SPI, SPI-MC-DG and SPI-MC penetrated and rearranged most fast compared with other complexes to a greater extent. That the *KP* and *KR* of the complex system increased slightly compared with SPI, implying that the conformation of the complex protein molecules changed slightly at the interface layer and exhibited better foaming properties. The *KP* of DG-MC-SPI (*KP* = 3.20) higher than SPI-MC-DG (*KP* = 3.11), suggesting that the introduction of MC and DG promoted the penetration also the rearrangement (compared with *KR*) of SPI at the air-water interface. Similar conclusion on foam properties was reported that protein molecules with high penetration rates and rapid rearrangement rates exhibited better foaming properties, which were more suitable for foaming agents (Cao, Xiong, Cao, & True, 2018).

4 Conclusion

We investigated the foam morphology of SPI, binary and ternary complexes. The results showed that the foams of ternary complexes were more uniform in size distribution compared with SPI in 1800 s evolution, among which SPI-MC-DG complex was most regular, indicating their excellent foam properties. Then, the FA and FS (Half-life time) at 25°C showed similar trends that SPI-MC binary and the ternary were significantly better than SPI, and other complexes whereas the ternary showed no significant FA except the SPI-MC and significantly differences in all complexes as the temperature rose. The surface dilatational rheology results illustrated that ternary and binary showed better foam properties especially the SPI-MC-DG and SPI-MC than SPI, which might because of the synergistic effect of MC on protein membrane elasticity improved the foaming properties of SPI. Therefore, to further expand its application in the food industry, the next stage of our work would investigate the feasibility of

SPI-MC-DG ternary complex as a carrier transport functional factor, further providing a theoretical basis for functional foods.

Declarations

Declaration of Competing Interest

The authors declare no conflict of interest.

Author Contribution

J. L. :Comceptualization, Methodology, Investigation, Formal analysis, Writing the main origin draft,Writing review & editing,Correspondence.D. L. :Investigation, Formal analysis, Validation, Visualization, Writing origin draft.Y.W.: Resourse, Validation.X.N.: Data curation, Formal analysis.S.L:Comceptualization, Supervision, Project administration, Funding acquisition, Writing review & editing,Correspondence.All authors reviewed the manuscript.

Acknowledgement

This work was supported by Outstanding Young and Middle-aged Science and Technology Innovation Team in Hubei Province(T2020012).

Data Availability

The raw data required to reproduce the findings of this study are available from the corresponding author upon reasonable request.

References

1. Azizi, R., Baggio, A., Capuano, E., & Pellegrini, N. (2024). Protein transition: focus on protein quality in sustainable alternative sources. *Critical Reviews in Food Science and Nutrition, 65*(18), 3401–3421. https://doi.org/10.1080/10408398.2024.2365339.
2. Bos, M. A., & Vliet, T. v. (2001). Interfacial rheological properties of adsorbed protein layers and surfactants: a review. *Advances in Colloid and Interface Science, 91*(3), 437–471. https://doi.org/10.1016/S0001-8686(00)00077-4.
3. Briceño-Ahumada, Z., & Langevin, D. (2017). On the influence of surfactant on the coarsening of aqueous foams. *Advances in Colloid and Interface Science, 244*, 124–131. https://doi.org/10.1016/j.cis.2015.11.005.

4. Cao, Y., Xiong, Y. L., Cao, Y., & True, A. D. (2018). Interfacial properties of whey protein foams as influenced by preheating and phenolic binding at neutral pH. *Food Hydrocolloids, 82*, 379–387. https://doi.org/10.1016/j.foodhyd.2018.04.020.
5. Dombrowski, J., Gschwendtner, M., & Kulozik, U. (2017). Evaluation of structural characteristics determining surface and foaming properties of β-lactoglobulin aggregates. *Colloids and Surfaces A: Physicochemical and Engineering Aspects, 516*, 286–295. https://doi.org/10.1016/j.colsurfa.2016.12.045.
6. Foegeding, E. A., Luck, P. J., & Davis, J. P. (2006). Factors determining the physical properties of protein foams. *Food Hydrocolloids, 20*(2–3), 284–292. https://doi.org/10.1016/j.foodhyd.2005.03.014.
7. Hu, J., Xu, H., Jiang, Z., & Hou, J. (2025). Air-water interfacial adsorption mechanism of whey protein/β-glucan complexes induced by phase behavior: Development of an emerging foaming agent. *Food Hydrocolloids, 167*. https://doi.org/10.1016/j.foodhyd.2025.111408.
8. Jian, M., Li, S., Zhu, Z., Zhang, N., Deng, Q., & Cravotto, G. (2023). Combination modes impact on the stabil ity of β-carotene-loaded emulsion constructed by soy protein isolate, β-glucan and myricetin ternary complex. *Food Research International, 172*, 113173. https://doi.org/10.1016/j.foodres.2023.113173.
9. Jin, Q., Li, X., Cai, Z., Zhang, F., Yadav, M. P., & Zhang, H. (2017). A comparison of corn fiber gum, hydrophobically modified starch, gum arabic and soybean soluble polysaccharide: Interfacial dynamics, viscoelastic response at oil/water interfaces and emulsion stabilization mechanisms. *Food Hydrocolloids, 70*, 329–344. https://doi.org/10.1016/j.foodhyd.2017.03.005.
10. Jin, W., Zhu, J., Jiang, Y., Shao, P., Li, B., & Huang, Q. (2017). Gelatin-Based Nanocomplex-Stabilized Pickering Emulsions: Regulating Droplet Size and Wettability through Assembly with Glucomannan. *Journal of Agricultural and Food Chemistry, 65*(7), 1401–1409. https://doi.org/10.1021/acs.jafc.6b04146.
11. Jurado Gonzalez, P., & Sörensen, P. M. (2020). Characterization of saponin foam from Saponaria officinalis for food applications. *Food Hydrocolloids, 101*. https://doi.org/10.1016/j.foodhyd.2019.105541.
12. Ke, C., & Li, L. (2024). Modification mechanism of soybean protein isolate-soluble soy polysaccharide complex by EGCG through covalent and non-covalent interaction: Structural, interfacial, and functional properties. *Food Chemistry, 448*. https://doi.org/10.1016/j.foodchem.2024.139033.
13. Kovalchuk, V. I., Aksenenko, E. V., Trukhin, D. V., Makievski, A. V., Fainerman, V. B., & Miller, R. (2018). Effect of Amplitude on the Surface Dilational Visco-Elasticity of Protein Solutions. *Colloids and Interfaces, 2*(4). https://doi.org/10.3390/colloids2040057.
14. Le, A. M., Erturk, M. Y., & Kokini, J. (2023). Effect of fat on non-linear rheological behavior of processed cheese spreads using coupled amplitude-frequency sweeps, Fourier Transform-

Chebyshev polynomials method, sequence of physical processes, and quantitative network analysis. *Journal of Food Engineering, 336*. https://doi.org/10.1016/j.jfoodeng.2022.111193.

15. Lei, D., Li, J., Zhang, C., Li, S., Zhu, Z., Wang, F., Grimi, N. (2022). Complexation of soybean protein isolate
16. with β-glucan and myricetin: Different affinity on 7S and 11S globulin by QCM-D and molecular simulation analysis. *Food Chemistry: X, 15*. https://doi.org/10.1016/j.fochx.2022.100426.
17. Li, J., & Li, L. (2025). Insight into the binding mechanism between soy protein isolate-oat β-glucan extrudate
18. and quercetin in nanoparticles by multi-spectroscopic techniques. *Food Chemistry, 471*. https://doi.org/10.1016/j.foodchem.2024.142723.
19. Li, X., Murray, B. S., Yang, Y., & Sarkar, A. (2020). Egg white protein microgels as aqueous Pickering foam stabilizers: Bubble stability and interfacial properties. *Food Hydrocolloids, 98*. https://doi.org/10.1016/.foodhyd.2019.105292.
20. Luo, F., Jian, M., Li, L., Xiao, J., Li, S., Zhang, N., & Zhu, Z. (2025). Stability and bioavailability of β-carotene-loaded emulsions improved by covalent interactions between soybean protein isolate, myricetin, and β-glucan. *International Journal of Biological Macromolecules, 332*. https://doi.org/10.1016/j.ijbiomac.2025.147912.
21. Maldonado-Valderrama, J., & Patino, J. M. R. (2010). Interfacial rheology of protein–surfactant mixtures. *Current Opinion in Colloid & Interface Science, 15*(4), 271–282. https://doi.org/10.1016/j.cocis.2009.12.004.
22. Musollini, S., Soukoulis, C., Tolve, R., You, L., Zanoni, M., Aprea, E., Favati, F. (2026). Viscoelastic characterisation of high protein ice cream: Predicting tactile sensory properties via time–concentration superposition and large amplitude oscillatory shear (LAOS) rheology. *Food Hydrocolloids, 172*. https://doi.org/10.1016/j.foodhyd.2025.112028.
23. Patino, J. M. R., Sánchez, C. C., Ortiz, S. E. M., Niño, M. R. R., & Añón, M. C. (2004). Adsorption of soy globulin films at the air–water interface. *Industrial & Engineering Chemistry Research, 43*(7), 1681–1689. https://doi.org/10.1021/ie0302443.
24. Peng, D., Jin, W., Li, J., Xiong, W., Pei, Y., Wang, Y., Li, B. (2017). Adsorption and Distribution of Edible Gliadin Nanoparticles at the Air/Water Interface. *Journal of Agricultural and Food Chemistry, 65*(11), 2454–2460. https://doi.org/10.1021/acs.jafc.6b05757.
25. Peng, D., Jin, W., Tang, C., Lu, Y., Wang, W., Li, J., & Li, B. (2018). Foaming and surface properties of gliadin nanoparticles: Influence of pH and heating temperature. *Food Hydrocolloids, 77*, 107–116. https://doi.org/10.1016/j.foodhyd.2017.09.026.
26. Peng, D., Yang, J., Li, J., Tang, C., & Li, B. (2017). Foams Stabilized by β-Lactoglobulin Amyloid Fibrils: Effect of pH. *Journal of Agricultural and Food Chemistry, 65*(48), 10658–10665. https://doi.org/10.1021/acs.jafc.7b03669.
27. Perez, A. A., Carrara, C. R., Sánchez, C. C., Santiago, L. G., & Rodríguez Patino, J. M. (2009). Interfacial dynamic properties of whey protein concentrate/polysaccharide mixtures at neutral pH.

Food Hydrocolloids, 23(5), 1253–1262. https://doi.org/10.1016/j.foodhyd.2008.08.013.

28. Pérez, O. E., Sánchez, C. C., Pilosof, A. M. R., & Rodríguez Patino, J. M. (2008). Dynamics of adsorption of hydroxypropyl methylcellulose at the air–water interface. *Food Hydrocolloids, 22*(3), 387–402. https://doi.org/10.1016/j.foodhyd.2006.12.005.
29. Rawel, H. M., Czajka, D., Rohn, S., & Kroll, J. (2002). Interactions of different phenolic acids and flavonoids
30. with soy proteins. *International Journal of Biological Macromolecules, 30*(3–4), 137–150. https://doi.org/10.1016/S0141-8130(02)00016-8.
31. Talansier, E., Loisel, C., Dellavalle, D., Desrumaux, A., Lechevalier, V., & Legrand, J. (2009). Optimization of dry heat treatment of egg white in relation to foam and interfacial properties. *LWT - Food Science and Technology, 42*(2), 496–503. https://doi.org/10.1016/j.lwt.2008.09.013.
32. Von Staszewski, M., Pizones Ruiz-Henestrosa, V. M., & Pilosof, A. M. R. (2014). Green tea polyphenols-β-lactoglobulin nanocomplexes: Interfacial behavior, emulsification and oxidation stability of fish oil. *Food Hydrocolloids, 35*, 505–511. https://doi.org/10.1016/j.foodhyd.2013.07.008.
33. Wan, Z., Yang, X., & Sagis, L. M. C. (2016a). Contribution of long fibrils and peptides to surface and foaming behavior of soy protein fibril system. *Langmuir, 32*(32), 8092–8101. https://doi.org/10.1021/acs.langmuir.6b01511.
34. Wan, Z., Yang, X., & Sagis, L. M. C. (2016b). Non-linear surface dilatational rheology and foaming behavior of protein and protein fibrillar aggregates in the presence of natural surfactant. *Langmuir, 32*(15), 3679–3690. https://doi.org/10.1021/acs.langmuir.6b00446.
35. Wang, Y.-L., Dai, S.-C., Lian, Z.-T., Cheng, X.-Y., Tong, X.-H., Wang, H., Jiang, L.-Z. (2024). Polyphenol improve the foaming properties of soybean isolate protein: Structural, physicochemical property changes and application in angel cake. *International Journal of Biological Macromolecules, 277*. https://doi.org/10.1016/j.ijbiomac.2024.134315.
36. Xiong, W., Ren, C., Jin, W., Tian, J., Wang, Y., Shah, B. R., Li, B. (2016). Ovalbumin-chitosan complex coacervation: Phase behavior, thermodynamic and rheological properties. *Food Hydrocolloids, 61*, 895–902. https://doi.org/10.1016/j.foodhyd.2016.07.018.
37. Yang, C., Wang, B., Wang, J., Xia, S., & Wu, Y. (2019). Effect of pyrogallic acid (1,2,3-benzenetriol) polyphe nol-protein covalent conjugation reaction degree on structure and antioxidant properties of pumpkin (Cucurbita sp.) seed protein isolate. *LWT - Food Science and Technology, 109*, 443–449. https://doi.org/10.1016/j.lwt.2019.04.034.
38. Yang, Q., Yang, J., Waterink, B., Venema, P., de Vries, R., & Sagis, L. M. C. (2024). Mung bean protein colloid mixtures and their fractions - A novel and excellent foam stabiliser. *Food Hydrocolloids, 155*. https://doi.org/10.1016/j.foodhyd.2024.110174.
39. Yang, W., Xu, C., Liu, F., Sun, C., Yuan, F., & Gao, Y. (2015). Fabrication Mechanism and Structural Characte ristics of the Ternary Aggregates by Lactoferrin, Pectin, and (−)-Epigallocatechin Gallate Using Multi spectroscopic Methods. *Journal of Agricultural and Food Chemistry, 63*(20), 5046–5054. https://doi.org/10.1021/acs.jafc.5b01592.

40. Zhan, F., Li, J., Shi, M., Wu, D., & Li, B. (2019). Foaming Properties and Linear and Nonlinear Surface Dilata tional Rheology of Sodium Caseinate, Tannin Acid, and Octenyl Succinate Starch Ternary Complex. *J ournal of Agricultural and Food Chemistry, 67*(8), 2340–2349. https://doi.org/10.1021/acs.jafc.8b06356.
41. Zhan, F., Li, J., Wang, Y., Shi, M., Li, B., & Sheng, F. (2018). Bulk, foam and interfacial properties of tannic acid/sodium caseinate nanocomplexes. *Journal of Agricultural and Food Chemistry, 66*(26), 6832–6839. https://doi.org/10.1021/acs.jafc.8b00503.
42. Zhan, F., Li, J., Youssef, M., & Li, B. (2021). Enhancement of foam stability parallel with foamability of the f oam stabilized by sodium caseinate-based complex: Octenyl succinate starch acting a dual role. *Food Hydrocolloids, 113*. https://doi.org/10.1016/j.foodhyd.2020.106479.
43. Zhao, M., Liu, L., Wang, G., Awais, M., Tong, L., Fan, B., Wang, F. (2024). Comparative study on the foam and air-water interface properties of ethanol-soluble and non-ethanol components in wheat aqueous phase protein. *Food Hydrocolloids, 150*. https://doi.org/10.1016/j.foodhyd.2023.109700.

Figures

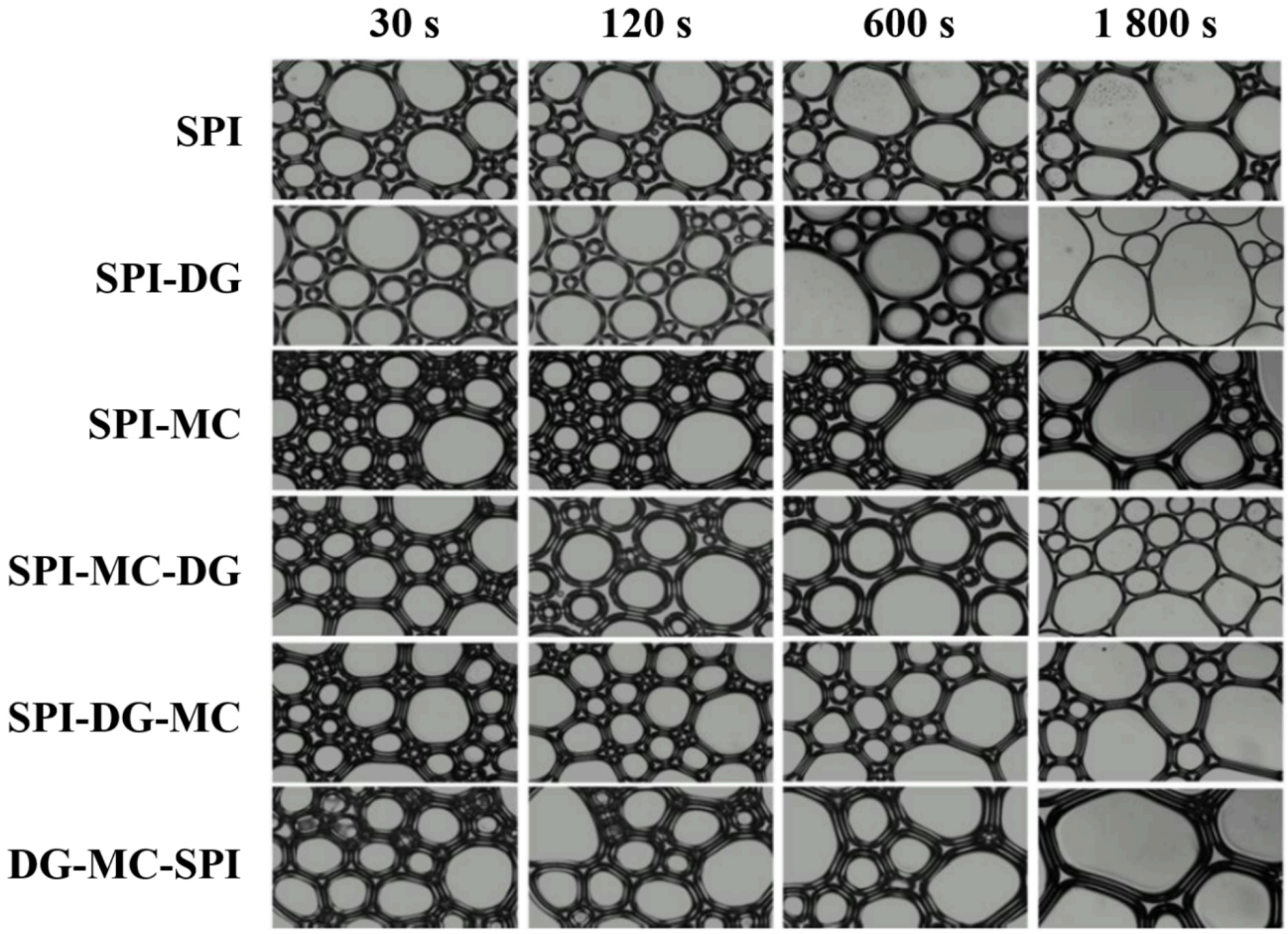


Figure 1

Scanning electron microscope images of bubble sizes of stabilized foams with different complexes system over time.

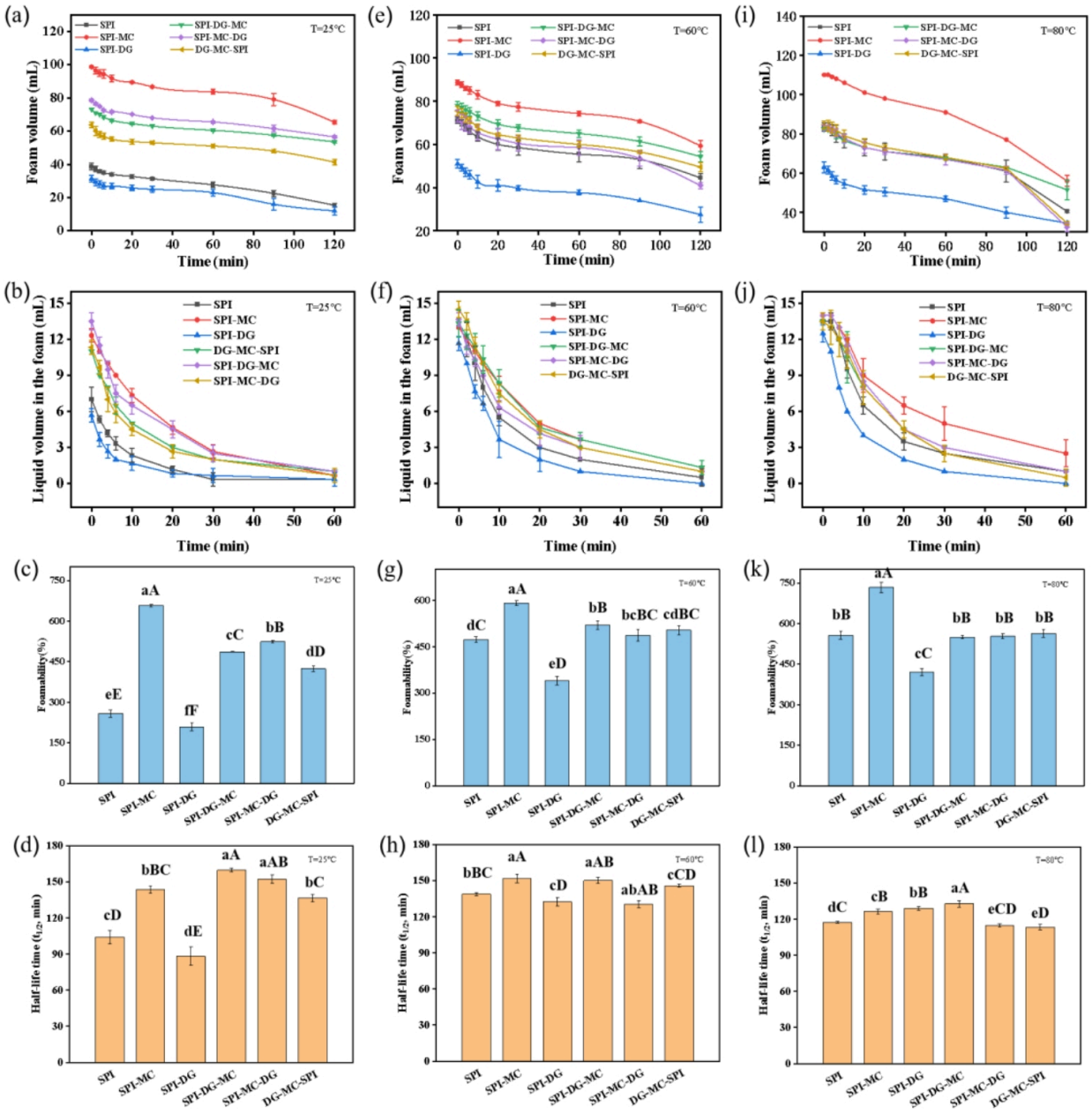


Figure 2

The Foam volume (a, e and i), liquid volume in the foam (b, f and j), FA (c, g and k) and half-life time (d, h and l) of complexes, respectively. a-e represent significant differences between different foam

ability/Half-life time at the $p<0.05$ level. A-E represent significant differences between different foam ability/Half-life time at the $p<0.01$ level.

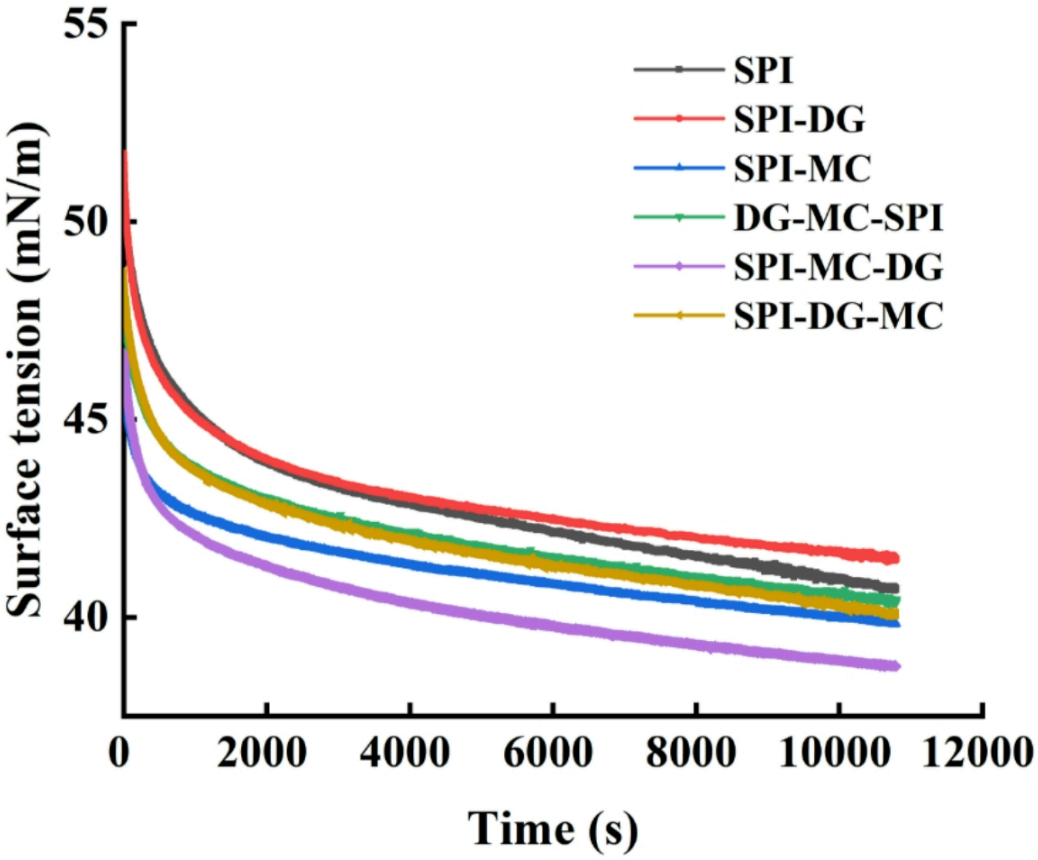


Figure 3

The surface tension curve of different complexes over time.

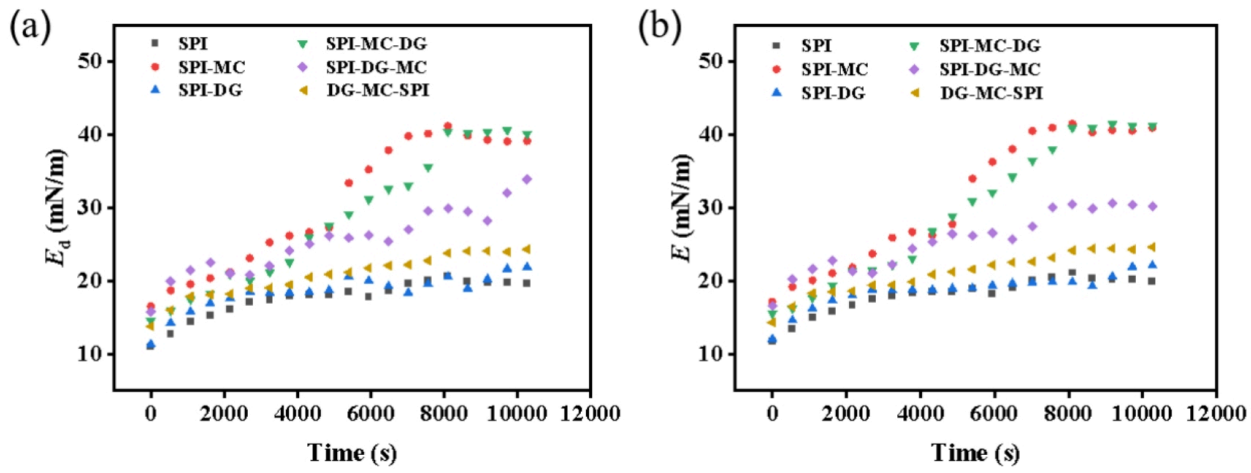


Figure 4

The curve of surface expansion modulus (a) and surface elastic modulus (b) of different composites with time (b).

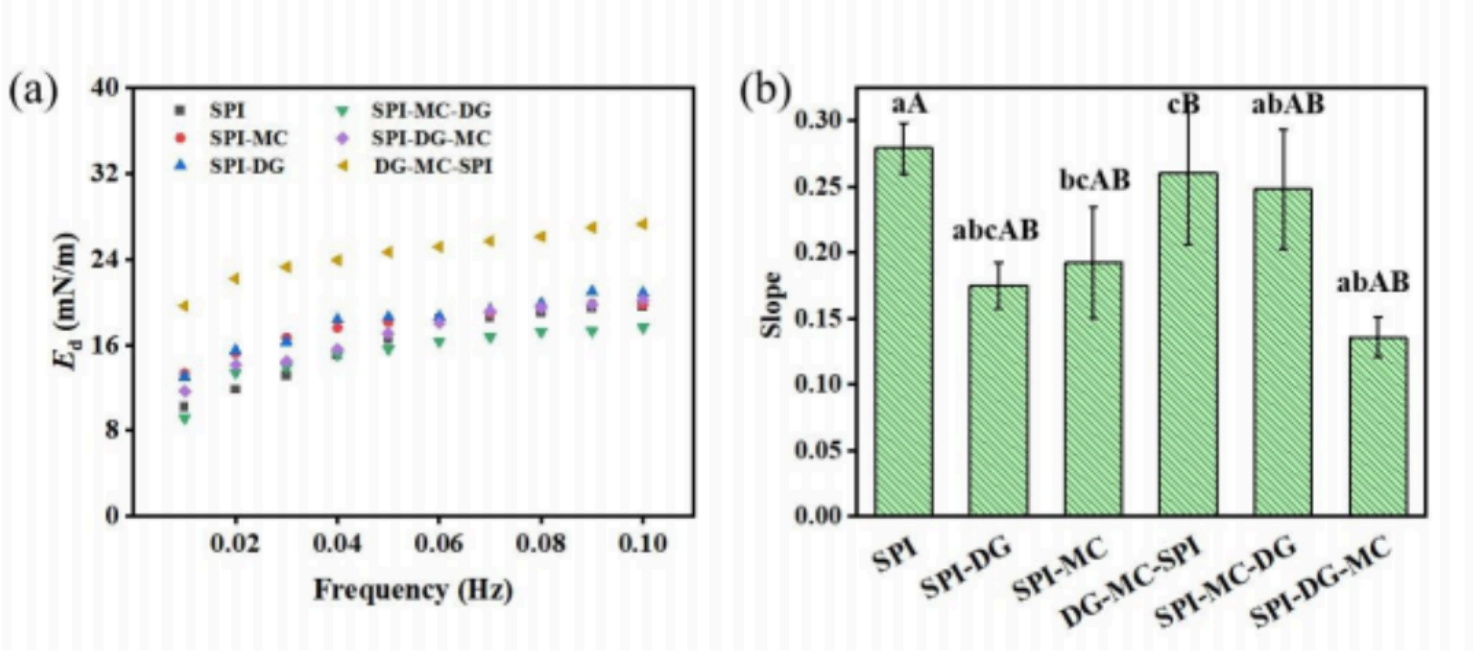


Figure 5

The surface expansion modulus of different complexes varies with frequency (a). Slope of double logarithm of surface expansion modulus and frequency of different complexes (b). a-c represent significant differences between different foam ability/Half-life time at the $p<0.05$ level. A-B represent significant differences between different foam ability/Half-life time at the $p<0.01$ level.

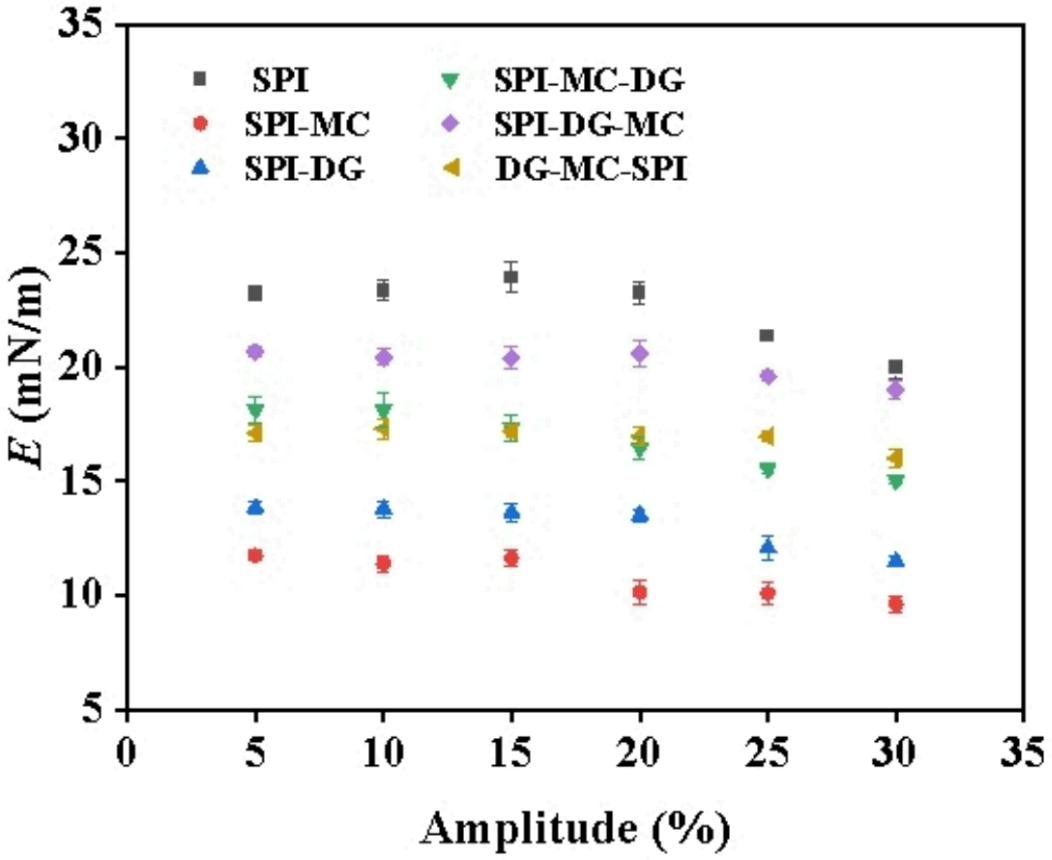


Figure 6

The surface expansion modulus of different complexes varies with amplitude.

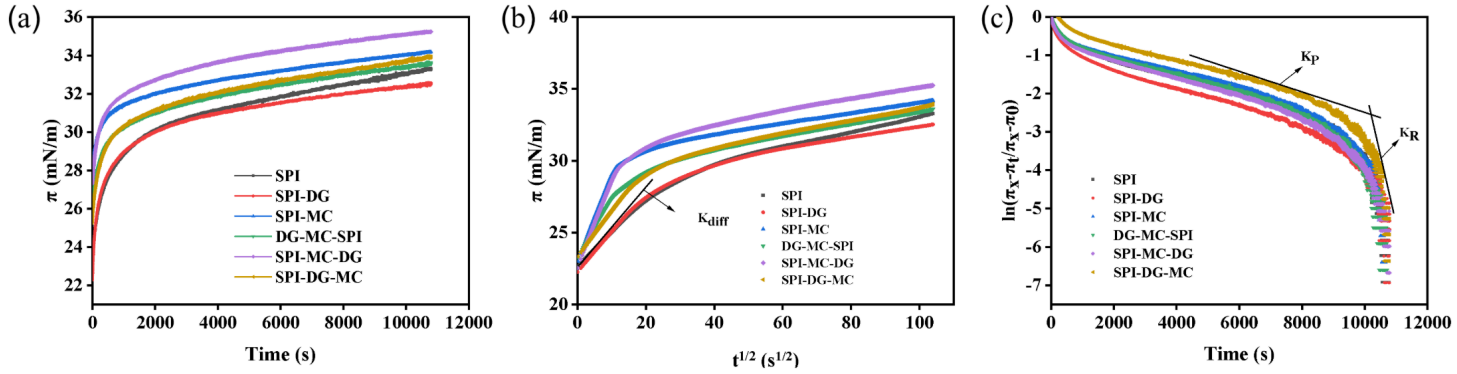


Figure 7

The curve of interfacial pressure (a) of different complexes. The curve of diffuse rate (*Kdiff*) (b), structure unfolding (*KP*) and rearrangement (*KR*) (c).